Dynamic modelling and vibration suppression of a single-link flexible manipulator with two cables

Lewei Tang, Marc Gouttefarde, Haining Sun, Lairong Yin, Changjiang Zhou

Dynamic modelling and vibration suppression of a single-link flexible manipulator with two cables

Lewei Tang[1, *], Marc Gouttefarde[2], Haining Sun[3], Lairong Yin[4], Changjiang Zhou[1, *]

1. State Key Laboratory of Advanced Design and Manufacturing for Vehicle Body, College of Mechanical & Vehicle Engineering, Hunan University, Changsha, 410082, China

2. LIRMM , University of Montpellier, CNRS, Montpellier, 34095, France

3. Department of Mechanical Engineering, Tsinghua University, Beijing, 100084, China

4. Key Laboratory of Safety Design and Reliability Technology for Engineering Vehicle, Changsha University of Science and Technology, 410004, PR China

Abstract

This paper introduces the dynamic modelling of a single-link flexible manipulator with two cables. The end-effector is attached at the distal end of the flexible link and tensed cables are used to suppress vibration. The flexible link is considered as Euler-Bernoulli beam and the cable as a massless spring. By applying the Hamilton's principle, a set of nonlinear equations of motion are derived with two boundary constraints. A calculation method is proposed to determine the natural frequency of the single-link flexible manipulator with cables. Simulation experiments are performed to validate the effectiveness of the proposed method. Three non-dimensional parameters are introduced to investigate the effect on the natural frequency of the flexible system. An experimental verification is implemented and the actual frequencies are found to be in good agreement with both the ones based on the proposed dynamic model and obtained in simulations. The results show that the vibration is greatly suppressed by utilizing cables in the flexible-link manipulator, which demonstrates that a light-weight flexible system with cables has the potential to be employed in the fields of fast lightweight industrial manipulators, robotic arms for remote manipulation in space and bio-inspired engineering.

Keywords: Single-link Flexible Manipulator; Dynamic Modelling; Cable; Vibration Suppression; Hamilton's Principle

Nomenclature

J_{m}	Moment of inertia of the motor
θ	Angular displacement of the motor
τ	Torque applied by the motor
EI	Bending stiffness of the flexible link
L	Length of the flexible link
ρ	Density per unit length
m_{l}	Link mass
m_{c}	Cable mass
m_{p}	Payload mass
J_{p}	Moment of inertia of the payload
D	Length of the rigid link
$o-xy$	Global inertial frame
$o-x'y'$	Tangential coordinate system (relative frame)
$\boldsymbol{r}_{\mathrm{rl}}$	Rigid displacement vector of a curvilinear point on the flexible link in the global inertia frame
s	Location of a curvilinear point on the flexible link
$v(s,t)$	Transversal deflection of a curvilinear point s on the flexible link
${}^{R}\boldsymbol{r}_{\mathrm{t}}$	Transversal deflection vector in the relative frame

$^{R}\boldsymbol{r}_{\mathrm{rl}}$	Rigid displacement vector of a curvilinear point on the flexible link in the relative frame
$\mathbf{T}$	Rotation matrix from the relative frame to the inertial frame
$V_{\mathrm{L}}, V_{\mathrm{C}}$	Potential energy of the flexible Euler-Bernoulli beam and the cable
λ	$= 1/L$
k	Spring constant of cables
ΔL	Change in the cable length
$V(s,t)$	Total potential energy of the single-link flexible manipulator with two cables
$T_{\mathrm{L}}, T_{\mathrm{P}}$	Kinetic energy of the flexible link and the tip mass payload
T	Total kinetic energy of the single-link flexible manipulator with cables
δW	Virtual work exerted by the rotational motor torque
$\Psi(s)$	Expression only related to the location of the curvilinear points s
$\omega_{i\_cable}, \omega_{i\_nocable}$	i^{th} natural frequency of the flexible link with cables and without cables
χ	$= \frac{\omega_{i\_cable} - \omega_{i\_nocable}}{\omega_{i\_nocable}}$
$d_{\mathrm{rtp}}, d_{\mathrm{rtp/c}}$	Relative distance between the location of the tip payload and the ideal location with cables and wit hout cables
$M_{\mathrm{p}},\ \Gamma_{\mathrm{p}},\ K$	Three non-dimensional parameters to illustrate the dynamic features of the flexible system

1. Introduction

Serial robotics with a set of rigid links have been widely employed in industrial application. However, the links of serial robots are generally relatively heavy and bulky in order to maintain high repeatability during motion. The dynamical motion of these robots is thus performed with a limited working speed due to large mass and inertia of bulky links. With the development of new materials and manufacturing technologies, flexible manipulators have attracted the interest of many researchers for the advantages of fast motions, large-scale manipulations and low manufacturing costs [1-6]. The compliance of flexible links can save energy, simplify the mechanical design and improve performance during a material manipulation. Except for fast lightweight industrial manipulators [7,8], potential applications of flexible manipulators include large space arms [9, 10] and bio-inspired systems with cables/soft appendages [11, 12].

The issue of developing accurate dynamic modelling of flexible link manipulators with rotational actuators had been studied by researchers over last 20 years [13-18], notably since the performance of model-based controllers highly depends on the accuracy of the dynamic modeling [19]. The flexible nature of a thin and slender link is considered by allowing a transversal deformation away from the predefined undeformed point as illustrated in Fig. 1. Regarding the flexible linkage modelling, there are two well-known approaches, namely Timoshenko beam theory [20] and Euler-Bernoulli beam theory [13,15,18,21,22]. In general, Euler-Bernoulli beam theory is broadly utilized under the assumption of neglecting both the shear deformation and rotary mass moment of inertia of the beam. Moreover, the governing equations of motion of a flexible link with tip mass is modeled with six methods in [23]. Besides, Lagrange equations [23], Newton-Euler equations [24, 25] and Hamilton's principle [13,16,18,26] were applied for developing a continuous dynamic model of a flexible link with tip mass. Rakhsha addressed the dynamic modelling of a single-link flexible robot with tip mass using Newton-Euler formulation, where natural frequencies and mode shapes were obtained by a simulation example in agreement with other literature [24]. The continuous dynamic model of the flexible link is obtained as Partial Differential Equations (PDEs) with several boundary conditions. The closed-form characteristic equation is deduced with PDEs of flexible links, which can be applied to study the relationships between design parameters and vibrations [15]. For flexible-link discrete models, the Finite Element Method (FEM) is employed to transform PDEs into Ordinary Differential Equations (ODEs) to investigate the characteristics of a flexible system in time and frequency domains [26, 27]. Besides, another method is the Assumed Mode Method (AMM) [28, 29] which consists in replacing the accurate mode shapes with several mode shapes of classical flexible beams (*e.g.* clamped-free flexible beams). In general, FEM with more degrees of freedom yields more precise results than AMM but requires more computation time. Therefore, AMM is preferable to FEM for real-time control purposes.

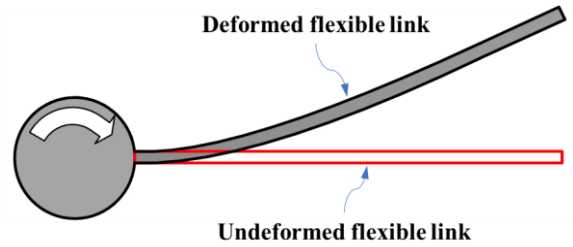

Fig 1. Bending effect of a flexible link.

The schematic of a single-link flexible manipulator with a gripper studied in the paper is shown in Fig. 2. A rotational motor is directly connected to the hub and a flexible link is clamped to the hub. A gripper, carrying a tip payload, is attached at the distal end of the link. Three types of manipulators, namely a single flexible-link flexible-joint manipulator, a single flexible-link rigid-joint manipulator and a single rigid-link flexible-joint manipulator, have been discussed by performing mode analysis in [16]. As for the flexible-link flexible-joint manipulator, the shaft connecting the motor and the hub is regarded as an ideal torsional spring. To study the influence of the stiffness of the flexible joint, a sensitivity index is proposed based on the closed-form characteristic equation of the system. The results showed that the joint flexibility has an important effect on the system frequencies [15]. For the sake of brevity, the effect of torsional shaft is neglected in the dynamic modelling of the single-link flexible manipulator studied in the present paper.

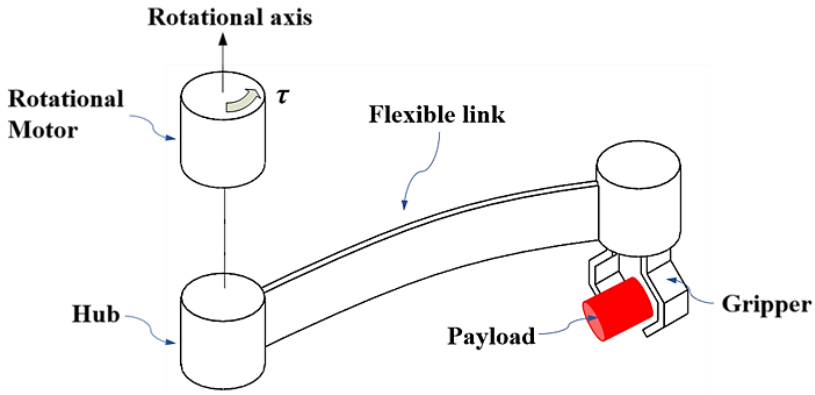

Fig 2. Schematic of a single -link flexible manipulator.

In the modelling of a flexible link, the curvilinear points on the flexible link are generally defined in relative coordinate systems. In kinematic analysis, two types of coordinate systems are referred to as Tangential Coordinate System (TCS) and Virtual Link Coordinate System (VLCS). Other coordinate systems are also discussed in [14] as pseudo-clamped, pseudo-pinned and pseudo-pinned-pinned systems, where pseudo-clamped reference frame is equivalent to TCS and pseudo-pinned-pinned to VLCS. The largest transversal deformation occurs at the distal end of flexible link in TCS, while it occurs near the middle of the link in VLCS. Additionally, the deformation of the flexible link at the distal end in VLCS is constrained at zero. In comparison, TCS is more intuitive and eases the modelling of the transversal deflection with constraint boundary conditions. Thus, TCS is adopted in this paper to facilitate the modeling of the single-link flexible manipulator under study.

Because of the flexibility of its slender links, a flexible single-link manipulator is hardly capable of displacing a payload within a good accuracy. With the aim to implement a light-weight manipulator, cables can be utilized to control the motion of the end-effector. In [9,10], ultra-long wings attached to satellites are considered as ultra-long spatial flexible structure, where vibrations along the flexible wings significantly influence the operation of the satellites. Cables are used to actively suppress the vibration of the flexible structure in the experiments. This type of cable actuated mechanism is defined as a Cable-driven Parallel Manipulator (CDPM). Among various studies related to CDPMs, *e.g.* [30, 31], a number of previous works dealt with the vibration analysis and suppression of CDPMs [32-39]. The dynamic stiffness matrix method is proposed in [33] to perform vibration analysis of CDPMs, which includes the dynamic characteristics of cables considering their masses. Cuvillon et al presented an active vibration damping method for CDPMs in frequency domain [34, 35]. Position control method is applied on winches to achieve dynamic control of a CDPM with elastic cables in [37]. Vibration control is investigated for redundant planar CDPMs in multi-axis reaction system for suppressing out-of-the-plane oscillations in [38]. Referring to [39], a cable is modelled as a massless linear axial spring for vibration analysis of CDPMs. However, all the aforementioned methods for vibration suppression focus on the rigid end-effectors without including the bending flexibility of the single-link manipulator. A feasible design to reduce the oscillations and enhance the stiffness of a flexible-link manipulator is to add cables between the flexible link and the hub [40]. Sun et al proposed in [9] a fuzzy PID control method with the aim of suppressing the vibrations of a flexible mechanism by means of four cables. The experiments show that the period of oscillation of the tip point is shorten quickly and the variation of the cable tensions is constrained in a predefined range. Besides, in [10], the dynamic model of a satellite with ultra-long wings and cables is presented on a basis of a flat-plate bending element with 12

degrees of freedom. Moreover, it is worth noting that in [9, 10] cables are also modelled as massless linear springs to analyze the dynamic response of spatial flexible structure to controllable force.

The main contribution of this paper is the dynamic modelling of a single-link flexible manipulator stiffened with cables, obtained by applying Hamilton's principle. The proposed dynamic model of single-link flexible manipulator with cables plays a crucial role in accurate motion control. Compared with finite element methods in [9,10,40], the presented dynamic modelling is systematic and results in a set of partial equations of motions and several boundary constraints. Compared to previous works on the dynamic modelling of a single-link flexible manipulator, the stiffening action of cables is accounted for in the dynamic model. Two testing experiments are setup to simulate a flexible manipulator made either of steel, aluminum, or copper, and both with and without cables. The resulting frequencies obtained from the simulations in two commercial softwares ANSYS and ADAMS are in good agreement with those based on the proposed modelling. Furthermore, the valuable effect of cables on vibration suppression of single-link manipulators is validated by comparing of relative distance of the link distal end point. The experimental verification of the dynamic model of the single-link flexible manipulator is also performed. Two types of flexible links made of steel or copper are tested with and without the action of cables. The resulting natural frequencies are obtained and compared with both the simulation results and the values obtained with the proposed model, in order to assess the effectiveness of the proposed dynamic modelling of a single-link flexible manipulator with cables.

The rest of this paper is organized as follows. The governing equations of motion are obtained as PDEs by the Hamilton's principle in Sect. 2. Natural frequency analysis is performed on the basis of this dynamic modelling in Sect. 3. Simulation experiments of the flexible-link manipulator are implemented both with and without cables, and the results are discussed in Sect. 4. Sensitivity analysis of natural frequency on three non-dimensional parameters is carried out in Sect. 5. The testbed is setup and experimental verification is implemented in Sect. 6 while Sect.7 concludes the paper.

2. Dynamic modelling

As illustrated in Fig. 3, the flexible manipulator is composed of a rotational motor, a flexible link, a rigid link, a payload and two cables. Let J_m, θ and τ denote the moment of inertia of the motor, the angular displacement of the motor and the torque applied by the motor. The shaft of rotational motor is fixed on the middle of the rigid link. The flexible link has bending stiffness EI, a length L with density per unit length ρ and uniform cross-section. The payload of mass m_p and moment of inertia J_p is attached to the distal end of the flexible link. The motion of the link is constrained in the horizontal plane. Moreover, its weight is ignored because the deformation due to the gravity is much smaller than the bending deformation of the flexible link. Cables are connected to the payload and the distal ends of the rigid link whose length is denoted $2D$. $o-xy$ frame denotes the global inertial frame of the single-link flexible manipulator. The relative frame $o-x'y'$ is a tangential coordinate system with the axis x' along the neutral axis of the undeformed link. Let θ denote the angular displacement of the flexible link with respect to the inertial frame.

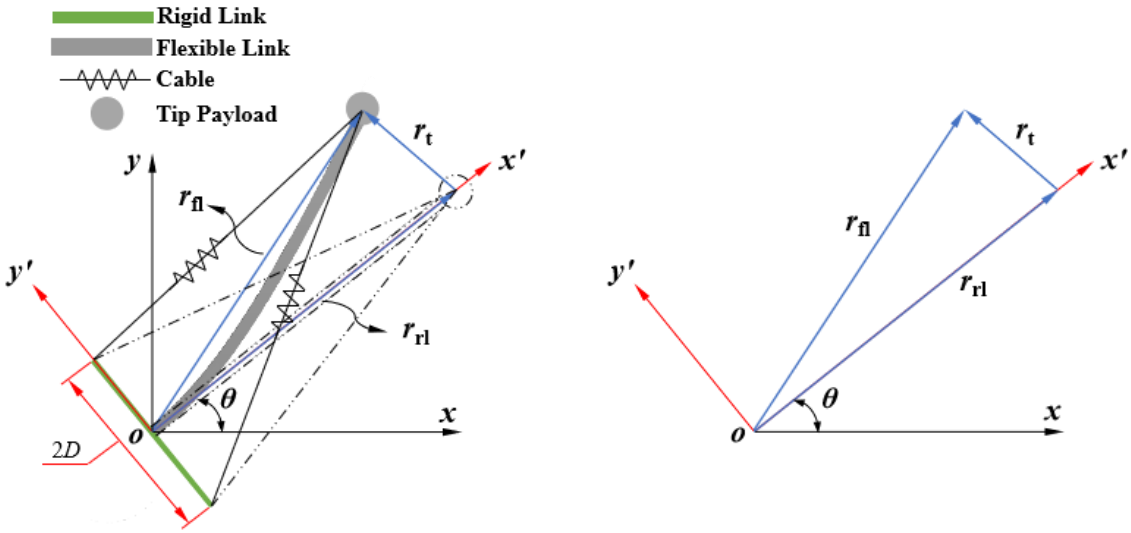

Fig. 3. Kinematic modelling of a single-link flexible manipulator with two cables.

The location of each curvilinear point on the flexible link is composed of a rigid location, corresponding to the undeformed link, and a transversal deflection due to the bending flexibility. The rigid displacement vector of a curvilinear point on the flexible link is expressed as $\boldsymbol{r}_{rl}$. The transversal deflection vector in the relative reference frame is denoted as ${}^{R}\boldsymbol{r}_t = [0, v(s,t)]^T$, which depends on the location of the curvilinear point s along the link and on time. Therefore, the location of the point on the link in the relative reference frame is obtained as

$$ {}^{R}\boldsymbol{r}_{\mathrm{fl}} = {}^{R}\boldsymbol{r}_{\mathrm{rl}} + {}^{R}\boldsymbol{r}_{\mathrm{t}}. \tag{1} $$

Let the original location of a curvilinear point of the flexible link in the inertial frame be denoted as $(s, 0)$. The rotation matrix from the relative frame to the inertial frame is expressed as

$$ \mathbf{T} = \begin{bmatrix} \cos\theta & -\sin\theta \\ \sin\theta & \cos\theta \end{bmatrix}. \tag{2} $$

Using Eqs. (1) and (2), the position vector in the inertial frame is given by

$$ \boldsymbol{r}_{\mathrm{fl}} = \begin{bmatrix} \cos\theta & -\sin\theta \\ \sin\theta & \cos\theta \end{bmatrix} \left(\begin{bmatrix} s \\ 0 \end{bmatrix} + \begin{bmatrix} 0 \\ v(s,t) \end{bmatrix} \right). \tag{3} $$

The potential energy of the system includes the potential energy of the flexible Euler-Bernoulli beam V_{L} due to bending, and the potential energy due to the extension of the cables. Under the assumption that the transversal deformation v is small, the potential energy of the link is given as

$$ V_{\mathrm{L}} = \frac{EI\lambda^3}{2} \int_0^1 \left(\frac{\partial^2 v}{\partial \zeta^2} \right)^2 d\zeta, \tag{4} $$

where $\lambda = 1/L, s = \zeta L,\ \zeta \in [0,1]$.

Moreover, following *e.g.* [10, 39], considering that each cable is a massless spring with spring constant k and assuming that only one cable is elongated at a given instant of time, the potential energy of the extended cable is

$$ V_{\mathrm{C}} = \frac{k}{2} \Delta L^2, \tag{5} $$

where ΔL denotes the change in the cable length and is equal to $\left| \sqrt{(v|_{s=L} + D)^2 + L^2} - \sqrt{D^2 + L^2} \right|$. Since the transversal deformation v is small, Eq. (5) is approximated as

$$ V_{\mathrm{C}} = \frac{kD^2}{2(D^2 + L^2)} v^2|_{s=L}. \tag{6} $$

Hence, the entire potential energy of the single-link flexible manipulator system with cables is expressed as

$$ V(s,t) = V_{\mathrm{L}} + V_{\mathrm{C}}. \tag{7} $$

The kinetic energy of the flexible link is given as

$$ T_{\mathrm{L}} = \frac{\rho L}{2} \int_0^1 \left(\frac{\partial \boldsymbol{r}_{\mathrm{fl}}}{\partial t} \right)^{\mathrm{T}} \left(\frac{\partial \boldsymbol{r}_{\mathrm{fl}}}{\partial t} \right) d\zeta\,. \tag{8} $$

Considering $s = \zeta L$, the following formulation is obtained from Eq. (3) as

$$ T_{\mathrm{L}} = \frac{\rho L}{2} \int_0^1 \left\{ \left(\frac{d\theta}{dt} \right)^2 [(\zeta L)^2 + v^2] + 2 \left(\frac{d\theta}{dt} \right) (\zeta L) \left(\frac{\partial v}{\partial t} \right) + \left(\frac{\partial v}{\partial t} \right)^2 \right\} d\zeta\,. \tag{9} $$

Furthermore, the kinetic energy of the tip mass payload is formulated as

$$ T_{\mathrm{P}} = \frac{m_{\mathrm{p}}}{2} \left(\frac{\partial \boldsymbol{r}_{\mathrm{fl}}}{\partial t}\bigg|_{s=L} \right)^{\mathrm{T}} \left(\frac{\partial \boldsymbol{r}_{\mathrm{fl}}}{\partial t}\bigg|_{s=L} \right) + \frac{J_{\mathrm{p}}}{2} \left(\frac{d\theta}{dt} + \frac{\partial^2 v}{\partial s \partial t}\bigg|_{s=L} \right)^2, \tag{10} $$

where $\frac{\partial^2 v}{\partial s \partial t}\Big|_{s=L}$ means the angular acceleration due the transversal oscillation of the tip payload. Therefore, the total kinetic energy of the system is deduced as

$$ T = \frac{1}{2} J_{\mathrm{m}} \left(\frac{d\theta}{dt} \right)^2 + T_{\mathrm{L}} + T_{\mathrm{P}}. \tag{11} $$

The virtual work exerted by the rotational motor torque is $\delta W = \tau \delta\theta$, which is the only work due to non-conservative generalized forces

for the single flexible link manipulator since the cables are modeled as springs.

In the following, the extended Hamilton's principle is applied to the single-link flexible manipulator as

$$\int_{t_1}^{t_2}(\delta T - \delta V + \delta W)dt = 0. \tag{12}$$

Using the principle of variation, the variation of the kinetic energy Eq. (11) can be written as follows

$$\delta T = J_{\mathrm{m}}\left(\frac{d^2\theta}{dt^2}\right)\delta\theta + \delta T_{\mathrm{L}} + \delta T_{\mathrm{P}}. \tag{13}$$

The last two terms in Eq. (13) are calculated as

$$\delta T_{\mathrm{L}} = \rho L\int_0^1\left\{[(\zeta L)^2 + v^2]\left(\frac{d^2\theta}{dt^2}\right)\delta\theta + v\left(\frac{d\theta}{dt}\right)\left(\frac{\partial v}{\partial t}\right)\delta\theta + \zeta L\left(\frac{\partial^2 v}{\partial t^2}\right)\delta\theta + \left[\zeta L\left(\frac{d^2\theta}{dt^2}\right) + v\left(\frac{d\theta}{dt}\right)^2 + \left(\frac{\partial^2 v}{\partial t^2}\right)\right]\delta v\right\}d\zeta\,, \tag{14}$$

$$\begin{aligned}\delta T_{\mathrm{P}} = {} & m_{\mathrm{p}}(L^2 + v^2|_{s=L})\left(\frac{d^2\theta}{dt^2}\right)\delta\theta + m_{\mathrm{p}}v|_{s=L}\left(\frac{\partial v}{\partial t}\right)\Big|_{s=L}\left(\frac{d\theta}{dt}\right)\delta\theta + m_{\mathrm{p}}\left(\frac{\partial v}{\partial t}\right)\Big|_{s=L}\delta\left(\frac{\partial v}{\partial t}\right)\Big|_{s=L} + m_{\mathrm{p}}L\left(\frac{d\theta}{dt}\right)\delta\left(\frac{\partial v}{\partial t}\right)\Big|_{s=L} \\ & + m_{\mathrm{p}}L\left(\frac{d^2\theta}{dt^2}\right)\delta v|_{s=L} + J_{\mathrm{p}}\left(\frac{d\theta}{dt} + \frac{\partial^2 v}{\partial s\partial t}\Big|_{s=L}\right)\left(\delta\frac{d\theta}{dt} + \delta\frac{\partial^2 v}{\partial s\partial t}\Big|_{s=L}\right).\end{aligned} \tag{15}$$

Subsequently, the variation of the potential energy in Eq. (7) is expressed as

$$\delta V = \delta V_{\mathrm{L}} + \delta V_{\mathrm{C}}. \tag{16}$$

All terms in Eq. (16) are formulated as

$$\delta V_{\mathrm{L}} = -EI\lambda^3\left[\left(\frac{\partial^2 v}{\partial\zeta^2}\right)\delta\left(\frac{\partial v}{\partial\zeta}\right)\Big|_{\zeta=0}^{\zeta=1} - \left(\frac{\partial^3 v}{\partial\zeta^3}\right)\delta v|_{\zeta=0}^{\zeta=1} + \int_0^1\frac{\partial^4 v}{\partial\zeta^4}\delta v\,d\zeta\right], \tag{17}$$

$$\delta V_{\mathrm{C}} = \frac{kD^2}{(D^2 + L^2)}v|_{s=L}\delta v|_{s=L}. \tag{18}$$

After several mathematical manipulations, the dynamic model is developed in combination with Eqs. (12) - (18) as follows

$$\begin{aligned}&\int_{t_1}^{t_2}A_1\delta\theta dt + \int_{t_1}^{t_2}\int_0^1 A_2\delta v\,d\zeta dt + \int_{t_1}^{t_2}A_3\delta\left(\frac{\partial v}{\partial s}\right)\Big|_{s=L}dt + \int_{t_1}^{t_2}A_4\delta v|_{s=L}dt \\ &\quad + \int_{t_1}^{t_2}\left(EI\left[\left(\frac{\partial^2 v}{\partial s^2}\right)\Big|_{s=0}\delta\left(\frac{\partial v}{\partial s}\right)\Big|_{s=0} - \left(\frac{\partial^3 v}{\partial s^3}\right)\Big|_{s=0}\delta v\Big|_{s=0}\right]\right)dt = 0.\end{aligned} \tag{19}$$

The terms A_i in Eq. (19) are given by

$$\begin{aligned}A_1 = {} & J_{\mathrm{m}}\left(\frac{d^2\theta}{dt^2}\right) + \tau + J_{\mathrm{p}}\left(\frac{d^2\theta}{dt^2} + \frac{\partial^3 v}{\partial s\partial t^2}\Big|_{s=L}\right) + m_{\mathrm{p}}(L^2 + v^2|_{s=L})\left(\frac{d^2\theta}{dt^2}\right) + \int_0^1\rho\zeta L^2\left(\frac{\partial^2 v}{\partial t^2}\right)d\zeta + m_{\mathrm{p}}L\left(\frac{\partial^2 v}{\partial t^2}\right)\Big|_{s=L} \\ & + \int_0^1\rho Lv\left(\frac{\partial v}{\partial t}\right)d\zeta\left(\frac{d\theta}{dt}\right) + m_{\mathrm{p}}v|_{s=L}\left(\frac{\partial v}{\partial t}\right)\Big|_{s=L}\left(\frac{d\theta}{dt}\right),\end{aligned}$$

$$A_2 = EI\lambda^3\frac{\partial^4 v}{\partial\zeta^4} + \rho L\left[\zeta L\left(\frac{d^2\theta}{dt^2}\right) + v\left(\frac{d\theta}{dt}\right)^2 + \left(\frac{\partial^2 v}{\partial t^2}\right)\right],$$

$$A_3 = EI\left(\frac{\partial^2 v}{\partial s^2}\right)\Big|_{s=L} + J_{\mathrm{p}}\left(\frac{d^2\theta}{dt^2} + \frac{\partial^3 v}{\partial s\partial t^2}\Big|_{s=L}\right),$$

$$A_4 = m_{\mathrm{p}} L\left(\frac{d^2\theta}{dt^2}\right) + m_{\mathrm{p}}\left(\frac{\partial^2 v}{\partial t^2}\right)\Big|_{s=L} - EI\left(\frac{\partial^3 v}{\partial s^3}\right)\Big|_{s=L} + \frac{kD^2}{(D^2+L^2)} v|_{s=L}. \tag{20}$$

The last term of Eq. (19) is always equal to zero due to the boundary conditions mentioned in Eq. (25) at $s = 0$. By taking into account that $\delta\theta, \delta v, \delta\left(\frac{\partial v}{\partial s}\right)\Big|_{s=L}$ and $\delta v|_{s=L}$ are independent variations, the expressions of A_1, A_2, A_3, and A_4 are equal to zeros on the basis of Eq. (19). Therefore, the dynamical model of a single-link flexible manipulator with cables is developed as

$$J_{\mathrm{m}}\left(\frac{d^2\theta}{dt^2}\right) + \tau + J_{\mathrm{p}}\left(\frac{d^2\theta}{dt^2} + \frac{\partial^3 v}{\partial s \partial t^2}\Big|_{s=L}\right) + m_{\mathrm{p}}(L^2 + v^2|_{s=L})\left(\frac{d^2\theta}{dt^2}\right) + \int_0^1 \rho\zeta L^2\left(\frac{\partial^2 v}{\partial t^2}\right) d\zeta + m_{\mathrm{p}} L\left(\frac{\partial^2 v}{\partial t^2}\right)\Big|_{s=L}$$
$$+ \int_0^1 \rho L v\left(\frac{\partial v}{\partial t}\right) d\zeta\left(\frac{d\theta}{dt}\right) + m_{\mathrm{p}} v|_{s=L}\left(\frac{\partial v}{\partial t}\right)\Big|_{s=L}\left(\frac{d\theta}{dt}\right) = 0, \tag{21}$$

$$EI\frac{\partial^4 v}{\partial s^4} + \rho\left[s\left(\frac{d^2\theta}{dt^2}\right) + v\left(\frac{d\theta}{dt}\right)^2 + \left(\frac{\partial^2 v}{\partial t^2}\right)\right] = 0, \tag{22}$$

$$EI\left(\frac{\partial^2 v}{\partial s^2}\right)\Big|_{s=L} + J_{\mathrm{p}}\left(\frac{d^2\theta}{dt^2} + \frac{\partial^3 v}{\partial s \partial t^2}\Big|_{s=L}\right) = 0, \tag{23}$$

$$m_{\mathrm{p}} L\left(\frac{d^2\theta}{dt^2}\right) + m_{\mathrm{p}}\left(\frac{\partial^2 v}{\partial t^2}\right)\Big|_{s=L} - EI\left(\frac{\partial^3 v}{\partial s^3}\right)\Big|_{s=L} + \frac{kD^2}{(D^2+L^2)} v|_{s=L} = 0, \tag{24}$$

with the boundary conditions at $s = 0$

$$v|_{s=0} = 0, \quad \frac{\partial v}{\partial s}\Big|_{s=0} = 0. \tag{25}$$

3. Natural Frequency Analysis

The dynamic characteristics of a single-link flexible manipulator include the natural frequency of the system in frequency domain and the dynamic response in time domain. Due to the small oscillation in free vibration, the lateral deformation $v(s,t)$ is assumed to be separable in space and time, which is given as below

$$v(s,t) = \Psi(s)\sin(\omega t) \tag{26}$$

where $\Psi(s)$ denotes an expression only related to the location s of the curvilinear points. By substituting of Eq. (26) into Eq. (22), the following equation is obtained

$$EI\frac{\partial^4 \Psi}{\partial s^4}\sin(\omega t) - \rho\Psi(s)\omega^2\sin(\omega t) = 0, \tag{27}$$

where $\frac{d\theta}{dt}$ is equal to zero when the motor stops rotating. Considering the generalized case, Eq. (27) leads to

$$EI\frac{\partial^4 \Psi(s)}{\partial s^4} - \omega^2\rho\Psi(s) = 0. \tag{28}$$

Let $\beta^4 = \omega^2\rho/EI$, then Eq. (28) can be written as

$$\frac{\partial^4 \Psi(s)}{\partial s^4} - \beta^4\Psi(s) = 0. \tag{29}$$

where the solution of this differential equation is given by $\Psi(s) = A\sin(\beta s) + B\cos(\beta s) + C\sinh(\beta s) + D\cosh(\beta s)$. (30)

Based on Eq. (30), Eqs. (23) to (25) are rewritten as

$$\left[-\rho\sin(\beta L)-J_{\mathrm{p}}\beta^3\cos(\beta L)\right]A+\left[J_{\mathrm{p}}\beta^3\sin(\beta L)-\rho\cos(\beta L)\right]B+\left[\rho\sinh(\beta L)-J_{\mathrm{p}}\beta^3\cosh(\beta L)\right]C$$
$$+\left[\rho\cosh(\beta L)-J_{\mathrm{p}}\beta^3\sinh(\beta L)\right]D=0. \tag{31}$$

$$\left[-m_{\mathrm{p}}\omega^2\sin(\beta L)+EI\beta^3\cos(\beta L)+\frac{kD^2}{(D^2+L^2)}\sin(\beta L)\right]A+\left[-m_{\mathrm{p}}\omega^2\cos(\beta L)-EI\beta^3\sin(\beta L)+\frac{kD^2}{(D^2+L^2)}\cos(\beta L)\right]B$$
$$+\left[-m_{\mathrm{p}}\omega^2\sinh(\beta L)-EI\beta^3\cosh(\beta L)+\frac{kD^2}{(D^2+L^2)}\sinh(\beta L)\right]C$$
$$+\left[-m_{\mathrm{p}}\omega^2\cosh(\beta L)-EI\beta^3\sinh(\beta L)+\frac{kD^2}{(D^2+L^2)}\cosh(\beta L)\right]D=0, \tag{32}$$

$$B+D=0, \tag{33}$$

$$A+C=0. \tag{34}$$

Subsequently, since $\delta\theta=0$, the first term of Eq. (19) is equal to zero and therefore Eq. (21) does not need to be considered. By using Eqs. (31) to (35), the coefficients A, B, C and D need to satisfy

$$\overbrace{\begin{bmatrix}H_{11}&H_{12}&H_{13}&H_{14}\\H_{21}&H_{22}&H_{23}&H_{24}\\0&1&0&1\\1&0&1&0\end{bmatrix}}^{\mathbf{\Pi}}\overbrace{\begin{bmatrix}A\\B\\C\\D\end{bmatrix}}^{\mathbf{x}}=\begin{bmatrix}0\\0\\0\\0\end{bmatrix}, \tag{35}$$

where

$$H_{11}=-\rho\sin(\beta L)-J_{\mathrm{p}}\beta^3\cos(\beta L),\ H_{12}=J_{\mathrm{p}}\beta^3\sin(\beta L)-\rho\cos(\beta L),$$
$$H_{13}=\rho\sinh(\beta L)-J_{\mathrm{p}}\beta^3\cosh(\beta L),\ H_{14}=\rho\cosh(\beta L)-J_{\mathrm{p}}\beta^3\sinh(\beta L),$$
$$H_{21}=-m_{\mathrm{p}}\omega^2\sin(\beta L)+EI\beta^3\cos(\beta L)+\frac{kD^2}{(D^2+L^2)}\sin(\beta L),$$
$$H_{22}=-m_{\mathrm{p}}\omega^2\cos(\beta L)-EI\beta^3\sin(\beta L)+\frac{kD^2}{(D^2+L^2)}\cos(\beta L),$$
$$H_{23}=-m_{\mathrm{p}}\omega^2\sinh(\beta L)-EI\beta^3\cosh(\beta L)+\frac{kD^2}{(D^2+L^2)}\sinh(\beta L),$$
$$H_{24}=-m_{\mathrm{p}}\omega^2\cosh(\beta L)-EI\beta^3\sinh(\beta L)+\frac{kD^2}{(D^2+L^2)}\cosh(\beta L).$$

For a non-trivial solution of vector **x** in Eq. (35), the determinant of matrix $\mathbf{\Pi}$ must be equal to zero. Thus, a nonlinear equation involving β is obtained by setting the determinant of matrix $\mathbf{\Pi}$ to be zero. In this paper, fzero function in Matlab is utilized to determine the resulting parameter β in the nonlinear equation. Once the parameter β calculated, the natural frequency ω can be determined according with $\beta^4=\omega^2\rho/EI$. For the purpose of illustration, values of the physical parameters of the single-link flexible manipulator are selected as shown in Tab. 1.

Table 1 Physical parameters of a flexible-link manipulator with Nylon cables (with the flexible link made of steel).

Item	Parameter	Value
Mass density (kg/m)	ρ	0.164
Link bending stiffness ($\mathrm{N\cdot m^2}$)	EI	0.1775
Link length (m)	L	0.6
Link mass (kg)	m_{l}	0.1
Motor moment of inertia ($\mathrm{kg\cdot m^2}$)	J_{m}	1×10^{-4}
Rigid link length (m)	D	0.1
Spring constant of cables (N/m)	k	3700

Cable mass (kg)	m_c	0.0005
Payload moment of inertia ($kg \cdot m^2$)	J_p	3.537×10^{-3}
Payload mass (kg)	m_p	0.01

To validate the proposed method, firstly the single-link flexible system without cables is considered by setting the cable spring constant k to zero. Consequently, the fundamental natural frequency of the single-link flexible manipulator without cables is obtained as 1.045 Hz by means of the proposed method. Referring to [24], an empirical formula for a flexible link with tip mass is utilized and the resultant fundamental natural frequency is calculated as

$$\omega_1 = \sqrt{\frac{3EI}{\left(m_p + \frac{33}{140}\rho L\right)L^3}} = 8.26 \text{ rad/s} = 1.372 \text{ Hz}. \tag{36}$$

Subsequently, a finite element simulation model of the flexible-link manipulator without cables is developed in ANSYS software. The frequency analysis is proceeded and the fundamental frequency is obtained as 1.033 Hz, which is very close to the result based on the proposed method with a relative error 1.16 %. In comparison, the relative error of the obtained fundamental frequency based on the empirical formula in Eq. (36) to that from ANSYS software is 32.8 %, which is much larger than the one obtained with the proposed method. Therefore, the results demonstrate that the proposed method for the flexible-link manipulator without cables is feasible and applicable. In addition, it provides the evidence that flexible link systems have a low natural frequency and are prone to vibrate due to external forces/moments. More importantly, the fundamental natural frequency of the single-link flexible manipulator with cables is determined as 2.724 Hz via the proposed method, which is nearly two times higher than that without cables. It means that cables can indeed be utilized as a structure element to increase the stiffness of a single-link flexible manipulator. In order to emphasize the effect of cables on this single-link flexible manipulator, the variations of the natural frequencies of the system with and without cables are listed in Tab. 2. As for the first two orders of natural frequencies of the single-link flexible manipulator, cables play an important role in improving the stiffness of the flexible system. However, it is also noted that the effect of cables on the higher order natural frequency decreases sharply as the order increases.

Table 2 Natural frequencies of flexible-link steel manipulator using the proposed method (Unit: Hz).

Order	Without cables	With cables
1st	1.045	2.724
2nd	3.124	6.935
3rd	13.11	14.38
4th	32.17	32.54
5th	60.13	60.29

To further investigate the influence of the link materials on the dynamic characteristics, two other commonly used materials (*i.e.*, copper and aluminum) are analyzed. The Elastic Modulus of steel, copper and aluminum are listed in Tab. 3.

Table 3 Elastic Modulus of steel, copper and aluminum (Unit: GPa).

Material	Plain Carbon Steel	Copper	Aluminum (1060 Alloy)
Elastic Modulus	207	110	69

The natural frequencies of the single-link flexible manipulator with both copper and aluminum are calculated and listed in Tab. 4. In comparison with the results in Tab. 2, the influence of materials on the natural frequencies of the single-link flexible manipulator is presented in Fig. 4.

Table 4 Natural frequencies of flexible-link manipulator with copper and aluminum (Unit: Hz).

Order	Without cables		With cables	
	Copper	Aluminum	Copper	Aluminum
1st	0.762	0.603	2.001	1.592
2nd	2.278	1.804	6.130	5.349
3rd	9.557	7.569	11.51	10.18
4th	23.45	18.57	23.99	19.31
5th	43.84	34.72	44.05	35.00

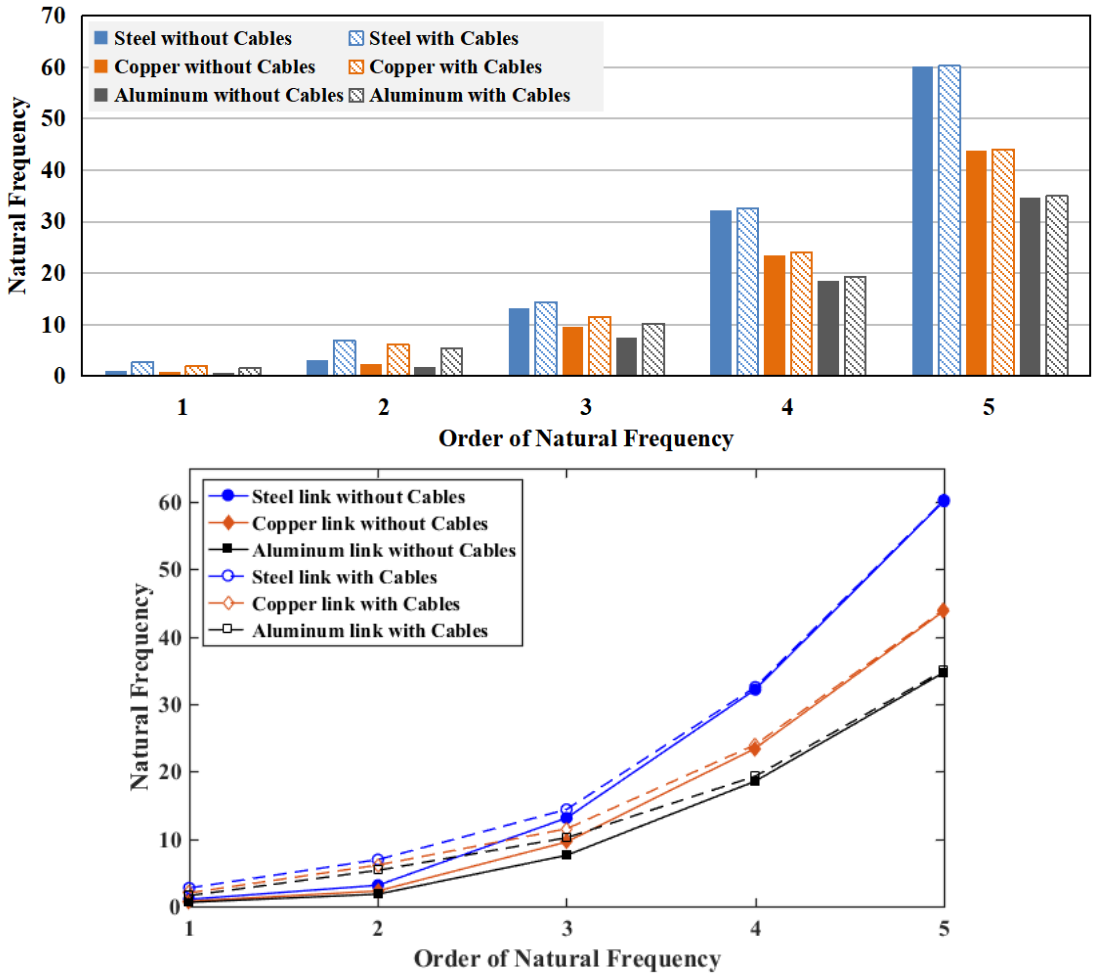

Fig. 4. Comparison of natural frequency of a single-link flexible manipulator made of steel/copper/aluminum with cables and without cables.

The calculation results show that the effect of cable decreases in high modes as shown in Fig. 4. Moreover, it validates the preceding remark that the cables have the ability to increase the stiffness of the flexible single-link manipulator with three commonly used metallic materials. In order to investigate the influence of cables on the dynamic characteristics of a flexible manipulator with different materials quantitatively, a non-dimensional index is defined as follows

$$\chi = \frac{\omega_{i\_cable} - \omega_{i\_nocable}}{\omega_{i\_nocable}}, \tag{37}$$

where ω_{i_cable} denotes the calculated i^{th} natural frequency using cables and $\omega_{i\_nocable}$ is the calculated i^{th} natural frequency without cables. Based on the values listed in Tabs. 3 and 4, the index values shown in Fig. 5 are obtained.

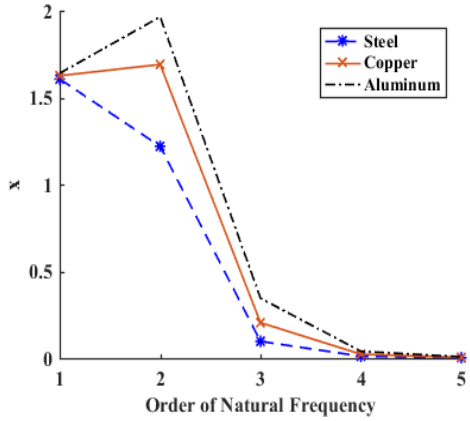

Fig. 5. Index values with three different material in the first five orders of natural frequency.

As represented in Fig. 5, the index is larger than zero throughout the first five orders of natural frequencies due to the improved stiffness of cables. The most significant influence of cables on the natural frequency occurs in the first and the second modes for all three materials. Moreover, cables exert more prominent effect on more flexible link and, therefore the values corresponding to aluminum are always higher than the values for the other two materials.

4. Simulation verification

Next, the effectiveness of the developed method for the steel single-link flexible manipulator with cables is investigated and verified by means of a simulation model developed in combination with ADAMS and ANSYS software as depicted in Fig. 6. The flexible link is discretized into 60 identical elements in two layers using ANSYS. A neutral file containing the features of the flexible link is obtained and transferred to ADAMS View. The reason for this process is that ADAMS View has a cable module to simulate the dynamics of cables in real environment. However, the modelling of the single link in ADAMS View is difficult to be created as a flexible structure. On the other hand, the flexible link model in ANSYS can be readily utilized to form the neutral file. Finally, the simulation of the single-link flexible manipulator with two cables can be achieved in combination with accurate cable model and flexibility of the single link. Moreover, the flexible link is mounted on the ground with a revolute joint. In practical application, the parallel cable configuration mentioned in [41-43] is capable of avoiding the torsion of the flexible link during transportation as shown in the right subfigure of Fig. 6.

Cables are modelled by employing the cable module in ADAMS View, where the diameter of the cables is set to 1 mm and the elastic modulus of the cables made of Nylon is 2.83 GPa. Referring to [40], the axial stiffness of an elastic cable with the constant cross-section and the same material is deduced as

$$k_{\text{ADAMS\_Cable}} = \frac{EA}{L} = 3704.5 \text{ N/m}, \tag{38}$$

which is approximately equal to the cable spring constant k in the proposed method. Furthermore, it is worth noting that both cables have zero tension in static condition where each cable has its free length.

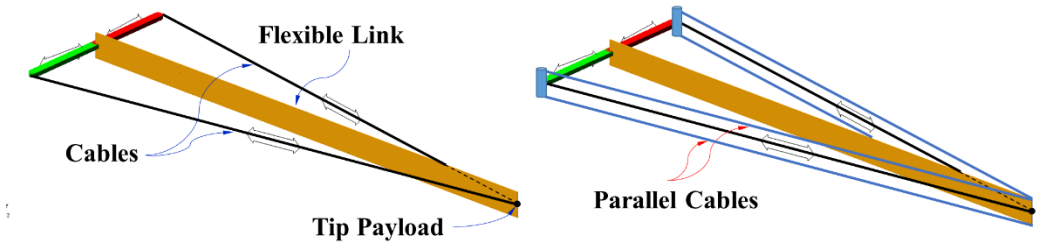

Fig. 6. Simulation model of flexible link with cables in ADAMS (left) and parallel cable configuration in practical engineering (right).

In the simulation experiment, the typical manipulation motion of the single-link flexible manipulator is divided into two sub-motions executed in sequence as illustrated in Fig. 7. In the first sub-motion, the manipulator rotates around the revolute joint from 0 to 90 degree in one second. Then, the revolute joint stops and the flexible manipulator is held in free vibration after time $t = 1$ s. The relative distance d_{rtp} between the simulated location of the tip payload and the ideal location of the tip payload in static condition is recorded during free vibration as shown in Fig. 8. Oscillations of the distal end of the flexible link can be clearly observed. Moreover, the relative distance d_{rtp} decays under the effect of the damping of both the cables and the flexible link, where the damping is added to the link and cable model in ADAMS. In free vibration of the steel flexible link with cables, the magnitude between crest and trough is measured as 0.297 mm for the first oscillation while it is 0.038 mm at the fifth oscillation. By taking the advantage of Fast Fourier Transform, the relative distance in time domain is transferred into the value in frequency domain as depicted in Fig. 9. Consequently, the fundamental frequency of the steel flexible-link manipulator with cables is identified as 2.715 Hz, which is very close to the value of 2.724 Hz calculated with the proposed dynamic model. The relative error between the simulation result and the calculated result on the fundamental frequency is 0.33 %. The main reason for the discrepancy is the simplified cable model considered in Section 2 (a spring with constant spring coefficient working only in extension).

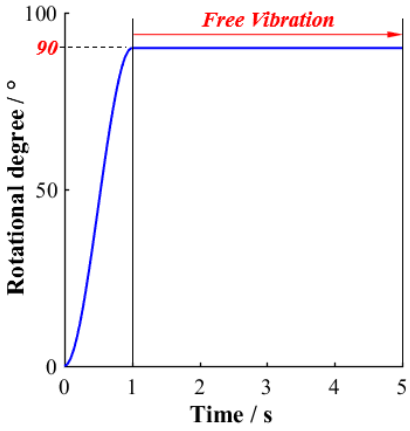

Fig. 7. Motion definition of simulation experiment.

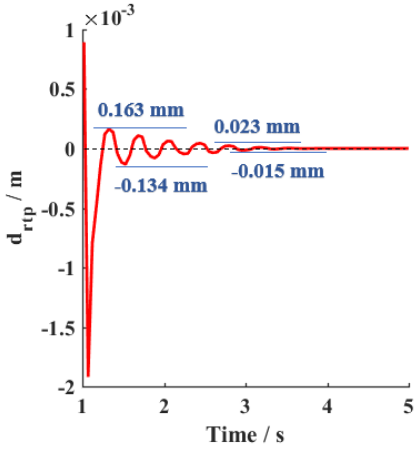

Fig. 8. Relative distance d_{rtp} in free vibration.

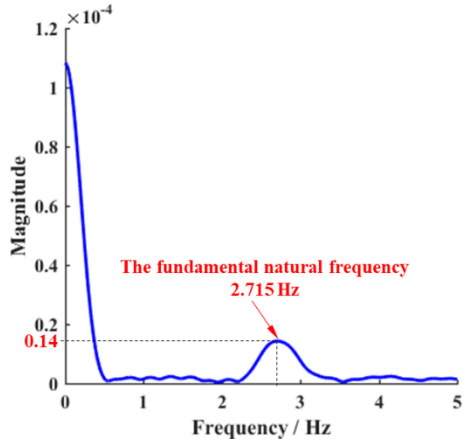

Fig. 9. Fast Fourier Transform of relative distance d_{rtp}.

Furthermore, the dynamic characteristics of the single-link flexible manipulator without cables are investigated by disabling the cable module in ADAMS. By completing the same motion of the revolute joint, the single-link flexible manipulator without cables vibrates freely. The relative distance $d_{\mathrm{rtp/c}}$ between the simulated and ideal (static conditions) locations of the tip payload is also measured in ANSYS as illustrated in Fig. 10. Compared to the relative distance d_{rtp} in Fig. 8, the amplitude of oscillations in free vibration of the flexible system without cables is much higher than that of the system with cables. Therefore, it confirms that the cables are capable of improving the stiffness of the flexible system and lowering the vibrations amplitude. Besides, the basic frequencies of the vibrations of flexible link made of steel/copper/aluminum are calculated as 1.057 Hz/ 0.756 Hz/ 0.625 Hz, which are in a good agreement with the calculated results.

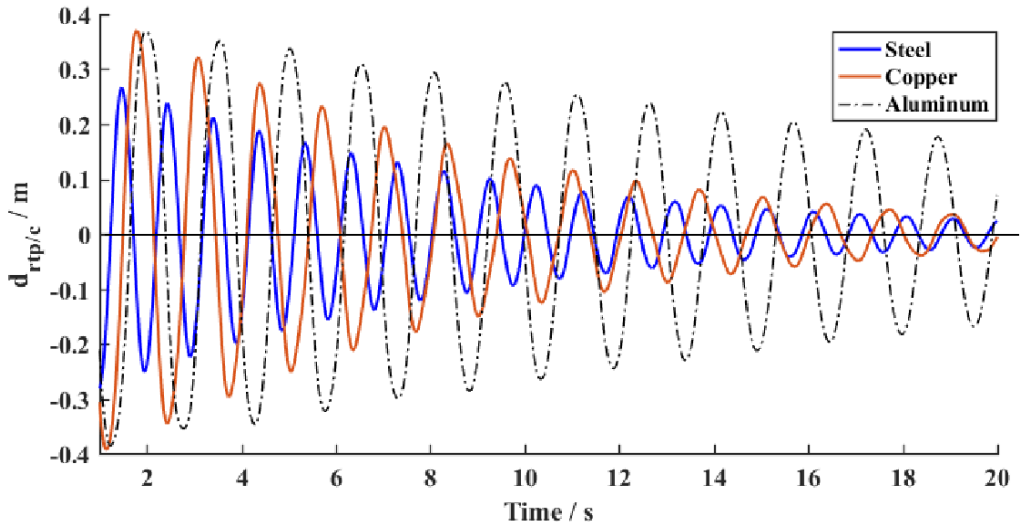

Fig. 10. Relative distance $d_{\mathrm{rtp/c}}$ in free vibration of the flexible manipulator without cables for three different materials.

In addition, the tensions in the two cables are also obtained from ADAMS and illustrated in Fig. 11. The dynamic features of this tension distribution along the defined motion are the following.

(1) During the simulation experiment, only one cable is maintained in tension and the other one is slack with tension equal to zero. For example, during the period I of the motion, only cable one is kept in tension (the dashed line in Fig. 11) and the tension of cable two remains zero (the solid line in Fig. 11), while during the period II**,** before the free vibration begins, only cable two is in tension and cable one stays slack. This feature is fully considered in the dynamic modelling of the flexible-link manipulator with only one cable having potential energy. During the period III of free vibrations, cables one and two are alternately tensed.

(2) Due to the effect of acceleration and deceleration during the revolute joint motion, the maximum tensions in cables one and two occur in period I and II, respectively. When the revolute joint stops rotating, the single-link flexible manipulator is experiencing the free vibration and the maximum magnitudes of the tensions in the two cables become smaller.

(3) During the free vibration, the tensile forces in each cable reduce over time. This feature is in agreement with the change of the relative distance d_{rtp} because of the spring model. Moreover, the cable tension acting on the flexible link is prone to be larger at the beginning of the exchange of working cable and decreases before next exchange of cable in action.

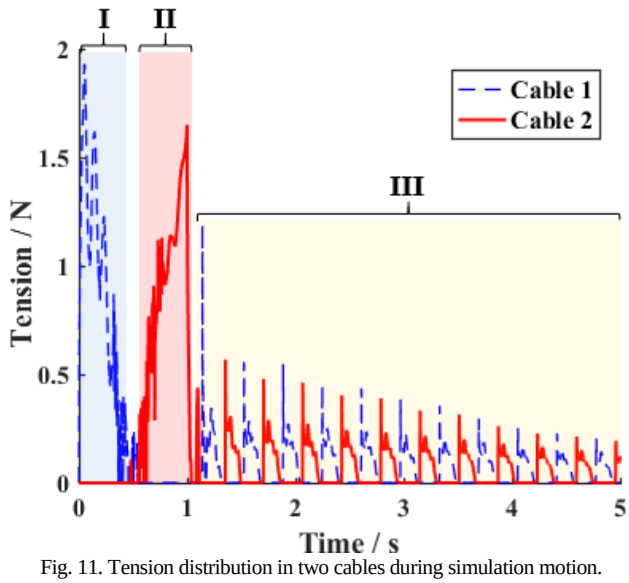

Fig. 11. Tension distribution in two cables during simulation motion.

5. Sensitivity Study

In order to investigate the dynamic characteristics especially in the frequency domain, sensitivity study is performed in this section. There are three main parameters having a crucial influence on the natural frequency of the flexible manipulator made of steel. Recalling the primary task of this flexible-link manipulator, the mass of the tip payload m_{p} and the moment of inertia of the tip payload J_{p} are two main factors leading to different dynamic features of the system. Moreover, cables are utilized as a spring module with spring coefficient k to increase the stiffness of the flexible system and the simulation results show its capability in suppressing vibrations. Therefore, three parameters including $\{m_{\mathrm{p}}, J_{\mathrm{p}}, k\}$ are taken into account in the sensitivity study presented in this section.

Referring to [15], three non-dimensional parameters are defined in the following and adopted to illustrate the dynamic features of the flexible system.

$$M_{\mathrm{p}} = \frac{m_{\mathrm{p}}}{\rho L},\ \ \Gamma_{\mathrm{p}} = \frac{J_{\mathrm{p}}}{\rho L^3},\ \ K = \frac{kL^3}{EI}. \tag{39}$$

Accordingly, the changes of the first three orders of natural frequencies are depicted with respect to three non-dimensional parameters $\{M_{\mathrm{p}}, \Gamma_{\mathrm{p}}, K\}$ in Fig. 12. The natural frequencies decrease as $\{M_{\mathrm{p}}, \Gamma_{\mathrm{p}}\}$ becomes larger. In contrast, the natural frequencies increase as K increases. More importantly, the results show that the fundamental natural frequency of the flexible system is highly related to the parameter Γ_{p}, while the second and the third natural frequencies mainly depends on the two parameters $\{M_{\mathrm{p}}, K\}$. Furthermore, the first natural frequency is more sensitive to the parameter Γ_{p} in the range of [0, 1] and the third natural frequency to the parameter M_{p} in the range of [0, 1].

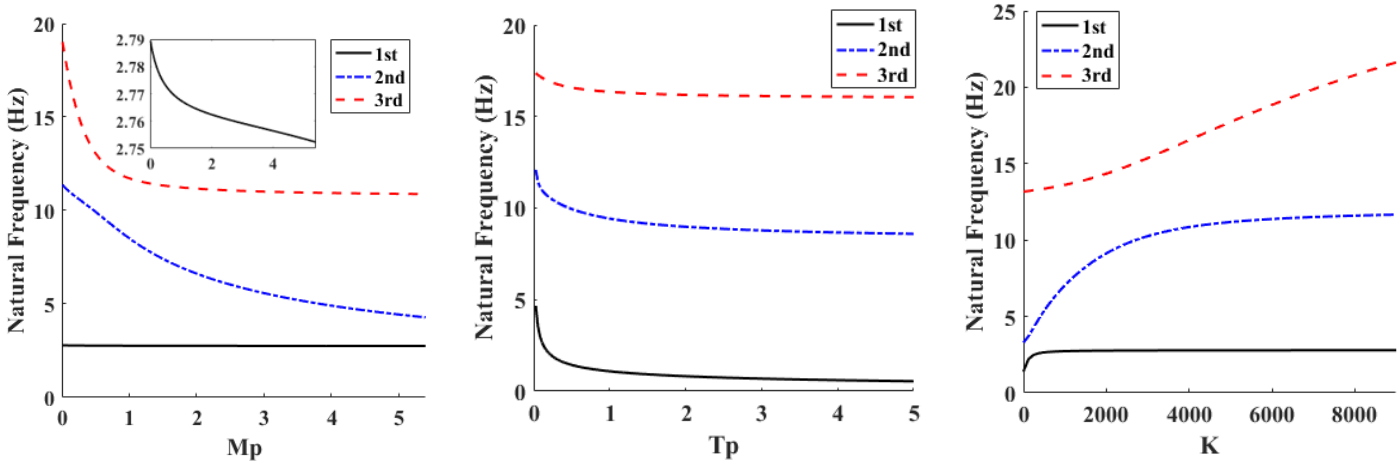

Fig. 12. Relationship of natural frequency and three non-dimensional parameters $\{M_{\mathrm{p}}, \Gamma_{\mathrm{p}}, K\}$.

6. Experimental Verification

In order to validate the proposed dynamic modelling, a testbed has been built. The layout of this experimental setup is shown in Fig. 13. It consists of a flexible link made of steel or copper connecting a servo motor via a hub, a payload attached at the tip of the flexible link, two cables connecting the payload and the hub, and a laser sensor fixed on the frame at one side of the link. The laser sensor is used to measure the distance of the tip end of the flexible link in the global frame during the vibrations. The physical parameters of the single-link flexible manipulator with two cables are given in Tab. 1 and Tab. 3. The experimental verification is implemented in two stages. Firstly, the free vibrations of the single-link flexible manipulators, made of steel or copper and without cables, are recorded as illustrated in Fig. 14. The corresponding fundamental natural frequencies are determined as 1.28 Hz (steel)/0.87 Hz (copper), which can be compared to the calculated theoretical values of 1.045 Hz (steel)/ 0.76 Hz (copper) obtained with the proposed dynamical model. The relative errors of the fundamental natural frequencies from the proposed model and the experimental results are 18.4% (steel)/ 12.6 % (copper), which demonstrates the effectiveness of the proposed dynamic modelling.

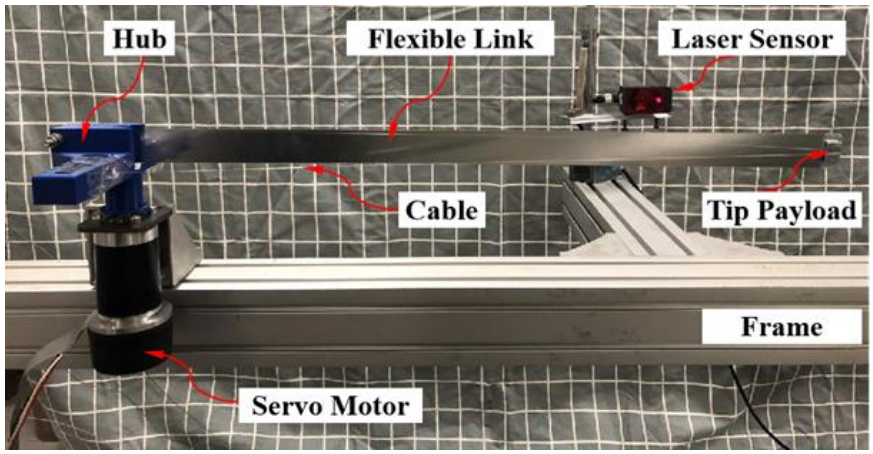

Fig. 13. Experimental setup of a single-link flexible manipulator with two cables.

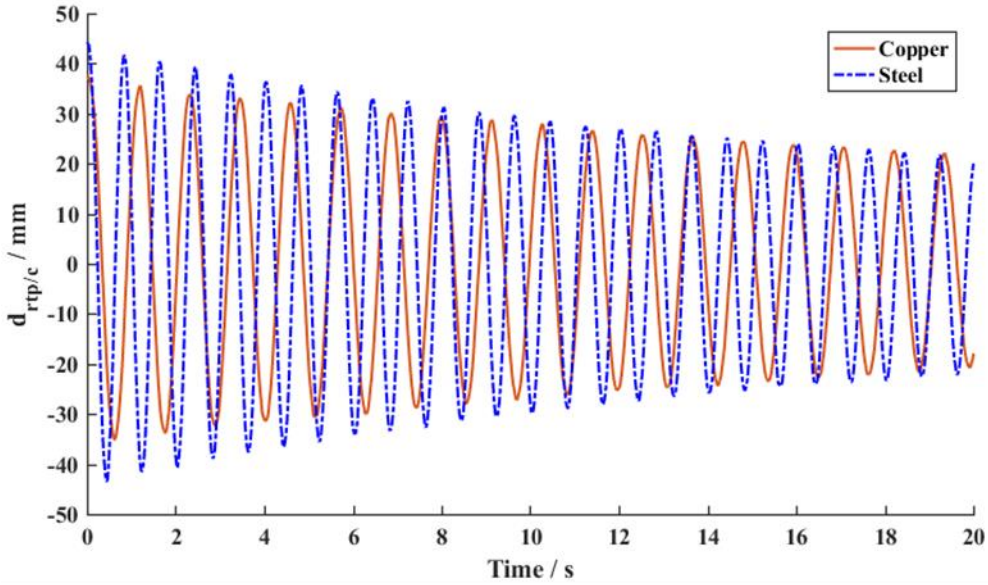

Fig. 14. Free vibration of the tip end of the single-link flexible manipulators made of steel/copper without cables.

Next, two cables are attached at the distal end of the flexible link. Following the same experimental procedure, the vibration of the distal end of the flexible link made of steel or copper are measured and recorded as shown in Fig. 15.

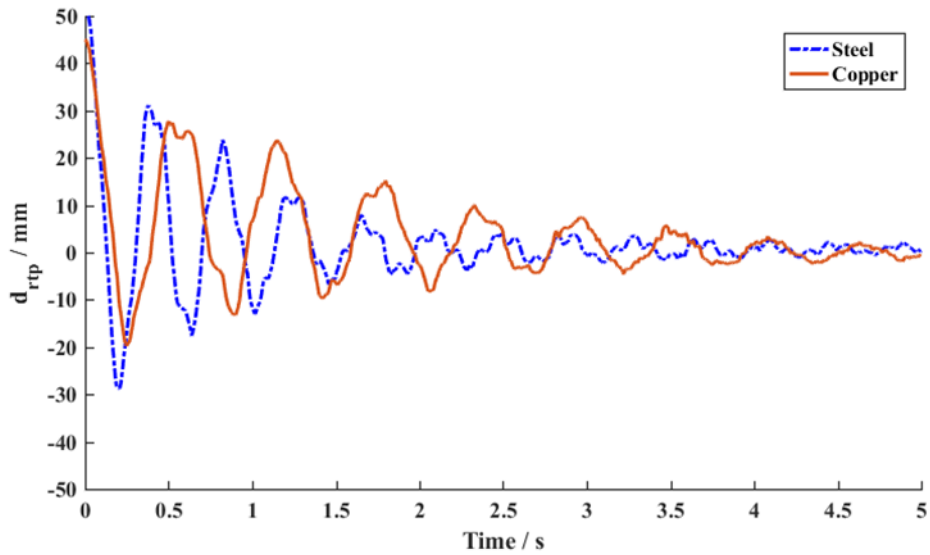

Fig. 15. Free vibration of the tip end of the single-link flexible manipulators made of steel/copper with cables.

Via Fast Fourier Transform, as presented in Fig. 16, the first two orders of natural frequencies of the link made of steel are identified as 2.42 Hz / 8.60 Hz while the theoretical values based on the proposed model are 2.72 Hz / 6.94 Hz as presented in Fig. 16. Regarding the copper link, the first two orders of natural frequencies are obtained as 1.71 Hz / 6.06 Hz while the theoretical values are calculated as 2 Hz/ 6.13 Hz. Overall, the natural frequencies of the same manipulators with cables are significantly higher than those without cables. It verifies that the cables exert a significant influence in improving the stiffness of the flexible link. It is also worth noticing that the vibration of the flexible manipulators with cables will be suppressed more quickly than that without cables, which are in accordance with the simulation results. Moreover, the differences between the actual frequencies and the values calculated with the proposed model may be caused by two aspects. During our experiments, it is found that the tensions in the cables directly influence the determination of the natural frequencies of the flexible link system. Thus, pre-tension in cables will lead to a higher frequency compared with the value from the proposed dynamic model. In addition, the cable tensions are not easy to measure accurately. Besides, the differences between experimental and theoretical values may be due to several assumptions made in the modelling. For example, the tip payload is considered to be attached in the middle of the tip of the flexible link in the proposed modeling, while the location of mass of the tip payload in the actual experiments did not fully meet this condition. In addition, there is a hub between the flexible link and the shaft of a servo motor, which may produce torsional flexibility into the dynamic model.

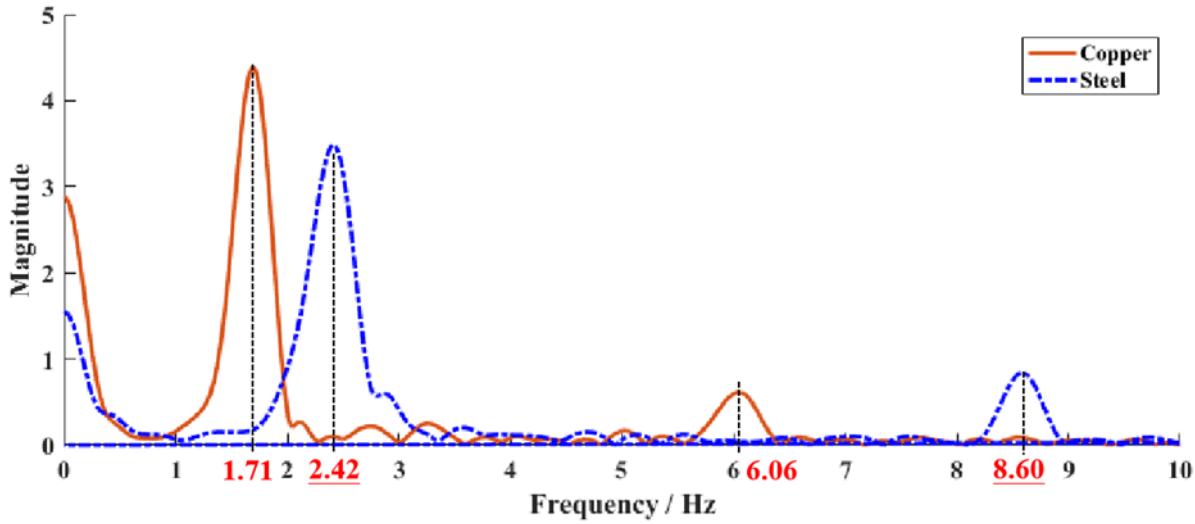

Fig. 16. Vibrations in frequency domain via Fast Fourier Transform.

7. Conclusions

In this paper, the dynamic modelling of a single-link flexible manipulator with two cables is presented, where the flexible link is modelled as Euler- Bernoulli beam and the cables as massless linear springs. The governing equations of motion are derived by utilizing Hamilton's

Principle, which yield a set of partial differential equations with corresponding boundary conditions. The natural frequencies of the single-link flexible manipulator with cables should satisfy the condition that the determinant of a defined matrix is equal to zero. The obtained fundamental natural frequency of the single-link flexible manipulator system without cables (obtained by setting the spring coefficient to zero) is validated by both the empirical equation and a finite element model in ANSYS. When considering the effect of cables on the flexible system, the resulting natural frequencies are higher than that of the system without cables, demonstrating that cables have the capability of enhancing the stiffness of the single-link flexible manipulator. Next, a combined simulation is setup to verify the effectiveness of the proposed dynamic model of the single-link flexible system with cables. The flexible link is developed into several elements in ANSYS, which is transferred to ADAMS. Cable module of ADAMS is employed to complete the simulation model. Then, a simulation of a basic motion is used to make the flexible link freely vibrate after one second. The simulation results show that the natural frequency with the proposed calculation method is very close to the value of the simulation experiment. The stiffening effect of the cables is verified by investigating the amplitudes of the oscillations in free vibration of the single-link flexible manipulator with and without cables. A sensitivity analysis is also made to investigate the effect of three dimensionless parameters on the natural frequencies of the flexible manipulator with two cables. Moreover, an experimental setup of a flexible link with cables has been built. The results in the experimental verification shows a relatively good agreement with the simulation and the values from the proposed dynamic model. This research is performed on a single-link flexible manipulator and lays the foundation of investigating the dynamic model of multiple-link flexible manipulator with cables. Moreover, further refinement of the proposed dynamic modelling and more precise cable tension measurements may be needed in order to more accurately predict the practical values of the natural frequencies.

Acknowledgments

This work is supported by the National Natural Science Foundation of China under Grant 52075153, the Fundamental Research Funds for the Central Universities and Natural Science Funds of Hunan Province in China under Grant 2018JJ3050.

References

1. Sun C, He W and Hong J. Neural network control of a flexible robotic manipulator using the lumped spring-mass model. *IEEE Transactions on Systems, Man and Cybernetics* 2017; 47(8):1863-1874.
2. Lochan K, Roy B and Subudhi B. A review on two-link flexible manipulators. *Annual Reviews in Control* 2016; 42:346-367.
3. Bascetta L, Ferretti G and Scaglioni B. Closed form Newton-Euler dynamic model of flexible manipulators. *Robotica* 2017; 35(5):1006-1030.
4. Xu W, Pan A and Ren H. Transferring optimal contact skills to flexible manipulators by reinforcement learning. *International journal of Intelligent robotics and applications* 2019; 3: 326-337.
5. Gao H, He W, Zhou C, et al. Neural Network control of a two-link flexible robotic manipulator using assumed mode method, *IEEE Transactions on Industrial Informatics* 2019; 15(2):755-765.
6. Liu Z, Liu J and He W. Dynamic modeling and vibration control for a nonlinear 3-dimensional flexible manipulator. *International journal of robust and nonlinear control* 2018; 28(13):3927-3945.
7. De Luca A, Siciliano B. Recursive Lagrangian Dynamics of Flexible Manipulator Arms. *IEEE Transactions on Systems, Man and Cybernetics* 1991; 21(4):826-839.
8. Meng Q, Lai X, Wang Y, et al. A fast stable control strategy based on system energy for a planar single-link flexible manipulator. *Nonlinear Dynamics* 2018; 94:615-626.
9. Sun H, Tang X, Wang X, et al. Vibration suppression of large flexible structure based on cable-driven parallel robots. *Journal of mechanical engineering* 2019; 55(11): 53-60.
10. Sun H, Tang, X, Cui Z, et al. Dynamic response of spatial flexible structures subjected to controllable force based on cable-driven parallel robots. *IEEE/ASME transactions on Mechatronics* 2020; 25(6):2801-2811.
11. Porez M, Boyer F, Belkhiri A. A hybrid dynamic model for bio-inspired soft robots: application to a flapping-wing micro air vehicle. *International Conference on Robotics and Automation (ICRA)* 2014:3556-3563.
12. Lau D, Oetomo D, Halgamuge S. Inverse Dynamics of Multilink Cable-Driven Manipulators with the Consideration of Joint Interaction Forces and Moments. *IEEE Transactions on Robotics* 2015; 31(2):479-488.
13. Zhu W and Mote CD. Dynamic modeling and optimal control of rotating Euler-Bernoulli beams. In: *Proceedings of the 1997 American Control Conference*, Albuquerque, NM, USA, 6 June 1997, paper no. 97CH36041, pp. 3110-3114. IEEE.
14. Oguamanam D, Bosnjak S and Zrnic N. On the dynamic modelling of flexible manipulators. *FME Transactions* 2006; 34:231-237.
15. Vakil M, Fotouhi R, Nikiforuk PN, et al. A study of the free vibration of flexible-link flexible-joint manipulators. *Proceedings of the Institution of Mechanical Engineers, Part C: Journal of Mechanical Engineering Science* 2011; 225:1361-1371.
16. Li D, Zu J and Goldenberg A. Dynamic modeling and mode analysis of flexible-link flexible-joint robots. *Mech. Mach. Theory* 1998; 33(7):1031-1044.
17. Dwivedy SK and Eberhard P. Dynamic analysis of flexible manipulators, a literature review. *Mech. Mach. Theory* 2006; 41(7):749-777.
18. Wei J, Cao D, Liu L, et al. Global mode method for dynamic modeling of a flexible-link flexible-joint manipulator with tip mass. *Applied Mathematical Modelling* 2017; 48:787-805.

19. Queiroz MS, Donepudi S, Burg T, et al. Model-based control of rigid-link flexible joint robot: an experimental evaluation. *Robotica* 1998; 16:11-21.
20. Salarieh H, Ghorashi M. Free vibration of Timoshenko beam with finite mass and flexural-torsional coupling. *J. Mech. Sci.* 2006; 38:763-779.
21. Hsu J, Lai H and Chen C. Free vibration of non-uniform Euler-Bernoulli beams with general elastically end constraints using Adomian modified decomposition method. *Journal of sound and vibration* 2008; 318(4-5):965-981.
22. Shahba A, Rajasekaran S. Free vibration and stability of tapered Euler-Bernoulli beams made of axially functionally graded materials. *Applied Mathematical Modelling* 2012; 36(7):3094-3111.
23. Piedœuf J. Six methods to model a flexible beam rotating in the vertical plane. In: *Proceeding of international conference on Robotics and Automation*, Seoul, Korea, 21-26 May 2001, paper no. 01CH37164, pp.2832-2839. IEEE.
24. Rakhsha F and Goldenberg A. Dynamics modelling of a single-link flexible robot. In: *Proceedings of international conference on Robotics and Automation*, St. Louis, USA, 25-28 March 1985, pp.984-989. IEEE.
25. Khalil W, Boyer F, Morsli F. General dynamic algorithm for floating base tree structure robots with flexible joints and links. *Journal of Mechanisms and Robotics* 2017, 9(3): 031003.
26. Tokhi M, Mohamed Z and Shaheed M. Dynamic characterisation of a flexible manipulator system. *Robotica* 2001, 19:571-580.
27. Damaren C, Sharf I. Simulation of Flexible-Link Manipulators with Inertial and Geometric Nonlinearities. *Journal of Dynamic Systems, Measurement and Control* 1995, 117(1): 74-87.
28. Al-Qaisia A and Al-Bedoor B. Evaluation of different methods for the consideration of the effect of rotation on the stiffening of rotating beams. *Journal of Sound and Vibration* 2005, 280:531-553.
29. Luca A, Siciliano B. Recursive Lagrangian Dynamics of Flexible Manipulator Arms. *IEEE Transactions on Systems, Man and Cybernetics* 1991, 21(4): 826-836.
30. Qian S, Bao K, Zi B, et al. Dynamic Trajectory Planning for a Three Degrees-of-Freedom Cable-Driven Robot Using Quintic B-splines. *Journal of Mechanical Design* 2020; 142(7): 073301(1-13).
31. Zhang Z, Shao Z, Peng F, et al. Workspace Analysis and Optimal Design of a Translational Cable-Driven Parallel Robot with Passive Springs. J*ournal of Mechanisms and Robotics* 2020; 12(5): 051005(1-14).
32. Caverly R. J and Forbes J. R. Dynamic modeling and noncollocated control of a flexible planar cable-driven manipulator. *IEEE Transactions on Robotics* 2014, 30(6): 1386-1397.
33. Yuan H, Courteille E, Gouttefarde M, et al. Vibration analysis of cable-driven parallel robots based on the dynamic stiffness matrix method. *Journal of Sound and Vibration* 2017, 394: 527-544.
34. Cuvillon L, Weber X, Gangloff J. Modal Controlfor Active Vibration Damping of Cable-Driven Parallel Robots. *Journal of Mechanisms and Robotics* 2020, 12(5): 051004.
35. Lesellier M, Cuvillon L, Gangloff J, et al. An active stabilizer for cable-driven parallel robot vibration damping. *2018 IEEE/RSJ International Conference on Intelligent Robots and Systems (IROS*), Oct 1-5, 2018, Madrid, Spain: 5063-5070.
36. Jamshidifar H, Khosravani H, Fidan B, et al. Vibration decoupled modeling and robust control of redundant cable-driven parallel robots. *IEEE/ASME Transactions on Mechatronics* 2018, 23(2): 690-701.
37. Begey J, Cuvillon L, Lesellier M, at al. Dynamic control of parallel robots driven by flexible cables and actuated by position-controlled winches. *IEEE Transactions on Robotics*, 2019, 35(1): 286-293.
38. Rushton M, Jamshidifa, Khajepour A. Multiaxis Reaction System (MARS) for Vibration Control of Planar Cable-Driven Parallel Robots. *IEEE Transactions on Robotics*, 2019, 35(4): 1039-1046.
39. Diao X, Ma O. Vibration analysis of cable-driven parallel manipulators. *Multibody System Dynamics*, 2009, 21(4): 347-360.
40. Dixit R and Kumar R. P. Cable stiffened flexible link manipulator. *2013 IEEE/RSJ International Conference on Intelligent Robots and Systems (IROS)*, September 14-18, 2014, Chicago, USA: 871-876.
41. Tang L, Shi P, Wu L, et al. Singularity analysis on a special class of cable-suspended parallel mechanisms with pairwise cable arrangement and actuation redundancy. *Journal of Mechanical Design*, 2020, 142(2): 024501.
42. Zhang Z, Shao Z, Wang L. Optimization and implementation of a high-speed 3-DOFs translational cable-driven parallel robot. *Mechanism and Machine Theory*, 2020, 145: 1-20.
43. Mottola G, Gosselin C, Carricato M. Dynamically feasible motions of a class of purely-translational cable-suspended parallel robots. *Mechanism and Machine Theory*, 2019, 132: 193-206.